Energy &
Environmental
Science

Electrolyte Design Implications of Ion-Pairing in Low-Temperature Li Metal Batteries

Journal:	*Energy & Environmental Science*
Manuscript ID	EE-ART-11-2021-003422.R1
Article Type:	Paper
Date Submitted by the Author:	08-Feb-2022
Complete List of Authors:	Holoubek, John ; University of California San Diego, Department of Nanoengineering Kim, Kangwoon; University of California San Diego, Program of Materials Science Yin, Yijie; University of California San Diego, Program of Materials Science Wu, Zhaohui; University of California San Diego, Department of Nanoengineering Liu, Haodong; University of California San Diego, Department of NanoEngineering Li, Mingqian; University of California San Diego, Program of Chemical Engineering Chen, Amanda ; University of California San Diego, Department of Nanoengineering Gao, Hongpeng; University of California San Diego, Program of Materials Science Cai, Guorui; University of California San Diego, Department of NanoEngineering Pascal, Tod; University of California San Diego, Department of NanoEngineering; University of California San Diego, Sustainable Power and Energy Center Liu, Ping; University of California San Diego, Department of NanoEngineering; University of California San Diego, Sustainable Power and Energy Center Chen, Zheng; University of California San Diego, Department of NanoEngineering; University of California San Diego, Sustainable Power and Energy Center

SCHOLARONE™
Manuscripts

Electrochemical kinetics and their temperature dependence play a vital role in the performance and environmental operating limitations of high-energy batteries. Technologically, the kinetic limitations of standard cell chemistries preclude the cycling of Li metal batteries at sub-zero temperatures, which suffer a severe reduction in reversibility of plating and stripping and catastrophic shorting events due to dendritic growth. The limitations of secondary batteries in these temperature ranges have been proposed to be limited by the ion-desolvation penalty faced by Li^+ at the electrolyte/electrode interphase, for which few methods of optimization exist. In this work, we demonstrate the importance of ion-pairing between Li^+ and the anion within the electrolyte to low-temperature operation through a systematic study. In doing so, we demonstrate homogenous Li metal deposition, highly-reversible plating and stripping, and hundreds of stable cycles in > 4 V Li metal full batteries down to -40 °C in an electrolyte system that would otherwise catastrophically fail under the same conditions without said ion-pairing in the solvation sphere. This work endeavors to unambiguously demonstrate the importance of solvation structure engineering in lithium battery electrolytes designed for operation under kinetic stress.

Electrolyte Design Implications of Ion-Pairing in Low-Temperature Li Metal Batteries

John Holoubek[a], Kangwoon Kim[b], Yijie Yin[b], Zhaohui Wu[c], Haodong Liu[a], Mingqian Li[c], Amanda Chen[c], Hongpeng Gao[b], Guorui Cai[a], Tod A. Pascal[a,b,c,d],*, Ping Liu[a,b,c,d],*, Zheng Chen[a,b,c,d],*

[a]*Department of NanoEngineering, University of California, San Diego, La Jolla, CA 92093, USA*

[b]*Program of Materials Science, University of California, San Diego, La Jolla, CA 92093, USA*

[c]*Program of Chemical Engineering, University of California, San Diego, La Jolla, CA 92093, USA*

[d]*Sustainable Power and Energy Center, University of California, San Diego, La Jolla, CA 92093, USA*

Abstract

Lithium metal batteries are capable of pushing cell energy densities beyond what is currently achievable with commercial Li-ion cells and are the ideal technology for supplying power to electronic devices at low temperatures ($\leq$ -20 ^{o}C). To minimize the thermal management requirements of these devices, batteries capable of both charging and discharging at these temperatures are highly desirable. Here, we report > 4 V Li metal full cell batteries (N/P=2) capable of hundreds of stable cycles down to -40 ^{o}C, unambiguously enabled by the introduction of cation/anion pairs in the electrolyte. Via controlled experimental and computational investigations in electrolytes employing 1,2-dimethoxyethane as the solvating solvent, we observed distinct performance transitions in low temperature electrochemical performance, coincident with a shift in the Li^+ binding environment. The performance advantages of heavily ion-paired electrolytes were found to apply to both cathode and anode, providing Li metal Coulombic efficiencies of 98.9, 98.5, and 96.9 % at -20, -40, and -60 ^{o}C, respectively, while improving the oxidative stability in support of > 4 V cathodes. This work reveals a strong correlation between ion-pairing and low-temperature performance while providing a viable route to Li metal full batteries cycling under extreme conditions.

Introduction

The advent of Li-ion batteries (LIBs) has enabled the rapid development of advanced portable electronics and electric vehicles. However, the application of existing and next-generation electronic devices in extremely low temperatures (< -20 ^{o}C) is currently limited by a significant reduction in the energy density of LIBs under such conditions.[1-5] Li metal batteries (LMBs), which replace the graphite anode (372 mAh g^{-1}) with Li metal (3860 mAh g^{-1}) have gathered recent interest to improve cell-level energy density, and if realized would be the ideal technology for low-temperature devices.[6] However, LMBs are known to face poor cycling stability due to the inherent reactivity and volume change of the Li metal anode. These factors present as a low Coulombic efficiency (CE) during repeated plating and stripping and may result in dendritic Li growth which may penetrate the battery separator and short the cell.[7,8] What's more, cycling of the Li metal anode under sub-zero conditions further exacerbate these effects.[9-11] To overcome these challenges, significant advancements in battery engineering and a scientific understanding of these devices and their temperature scaling is crucial.

42   To address the capacity and voltage loss experienced by secondary batteries at low
43   temperature, engineering of the electrolyte chemistry has emerged as a promising tool.[8-16] Though
44   there has been much progress in the improvement of low temperature battery performance, most
45   works have focused on the improvement of low temperature discharge following a charge at
46   benign temperatures. [2,4,15,16] Unless the device employing such batteries can be removed from the
47   cold operating environment during charge, this operation protocol inherently couples the designed
48   battery to an external warming device. These warming systems consume non-negligible power and
49   contribute mass to the overall system, thus reducing overall operating efficiency and energy
50   density.[17,18] For applications that must be charged in their working environment, enabling low
51   temperature charge and discharge is necessary to reduce or eliminate the need for thermal
52   management at low temperature. For LMBs, this implies that Li metal must be reversibly plated
53   and stripped under these conditions.

54   Along with technological progress, a more rigorous understanding of the interplay between
55   various limiting factors at low temperature is necessary. Historically, improving the bulk ionic
56   conductivity, solid-electrolyte interphase (SEI) composition, and Li^+ charge-transfer penalty have
57   been the foremost goals of low temperature electrolyte design.[3,4, 9-11,19-21] Among these factors, it
58   has been suggested that the charge-transfer penalty is the dominant limitation among systems with
59   sufficient bulk transport.[2,22,23] However, the heterogenous charge-transfer process in
60   electrochemical systems is invariably complicated, particularly given that there is no mechanistic
61   consensus regarding Li^+ dynamics at the electrode interphase in the presence of a SEI. While it is
62   clear that factors such as SEI composition, Li^+ solvation structure, and interphasial dynamics play
63   important roles in this process, their influence on one another is largely unknown. Hence, the
64   technological advancement of temperature-resilient energy storage is heavily linked to a
65   fundamental understanding of the charge-transfer process.

66   Our previous work aimed to provide low temperature system design principles based on
67   the hypothesis that the solvation environment of the Li^+ ion in the electrolyte defines the charge-
68   transfer barrier and its temperature dependence.[23] While we demonstrated state-of-the art Li metal
69   reversibility down to -60 ºC, the design insights gleaned from the LMB electrolyte of interest
70   raised many questions that have yet to be answered. It was concluded that solvents of weak Li^+
71   binding were crucial to advantageous temperature scaling of Li metal reversibility, which agrees

72 with the results from Li et al.[22], Fan et al.[16], and Wang et al.[24]. However, such weak binding

73 solvents commonly result in Li^+/anion binding in bulk solution, making a direct correlation

74 between low temperature performance and any one factor difficult. This work aims to decouple

75 the influence of ion-pairing and Li^+/solvent binding energy to gain a more definitive sub-zero LMB

76 electrolyte design rationale and provide further insights on the temperature dependence of charge-

77 transfer.

78   To provide such data, we propose a detailed comparison of electrolytes composed of the

79 same solvating solvent with varying degrees of ion-pairing. The most direct way to accomplish

80 this would be varying the solvating solvent/Li salt ratio.[25-27] However, the high viscosity of such

81 electrolytes make this untenable when scaling to low temperatures, where any advantage in

82 interphasial charge-transfer kinetics would be completely obscured by the overwhelming decrease

83 in ionic conductivity.[16] Fortunately, a solution to this already exists in the advent of localized

84 high-concentration electrolytes (LHCEs). These systems apply diluent solvents, which interact

85 weakly with Li^+ and dissolve negligible salt on their own, in order to reduce the bulk viscosity of

86 high-concentration electrolytes.[28-30] In doing so, any effects of ion-pairing in the Li^+ solvation

87 shell can be decoupled from the bulk ionic conductivity of the solution at low temperature. LHCEs

88 employing 1,2-dimethoxyethane (DME) was chosen as the primary basis of this investigation. This

89 solvent has been well established to provide reversible room temperature Li metal performance

90 when paired with lithium bis(fluoro sulfonyl)imide (LiFSI), even at dilute concentrations.

91 However, the temperature dependence of Li reversibility is demonstrably acute[23,31,32], which we

92 and others have proposed to be linked to its strong binding with Li^+. Thus we pair the LiFSI/DME

93 components with a bis(2,2,2 trifluoro ethyl)ether (BTFE) diluent, which allows for the modulation

94 of the degree of ion-pairing while maintaining a relatively low bulk viscosity. We incrementally

95 alter the BTFE/DME volume ratio from 1 M LiFSI in pure DME to 1 M LiFSI BTFE/DME (7:1,

96 8 M equivalent local concentration). Using both theoretical and experimental methods, we

97 demonstrate that there is a distinct ion-pairing transition when the local concentration exceeds 4

98 M (3:1 BTFE/DME ratio), which results in vastly improved Li metal performance at low

99 temperatures, while improving the oxidative stability and thus enabling the implementation of

100 $LiNi_{0.8}Mn_{0.1}Co_{0.1}O_2$ (NMC 811) as a cathode material. This concept was utilized to design LMBs

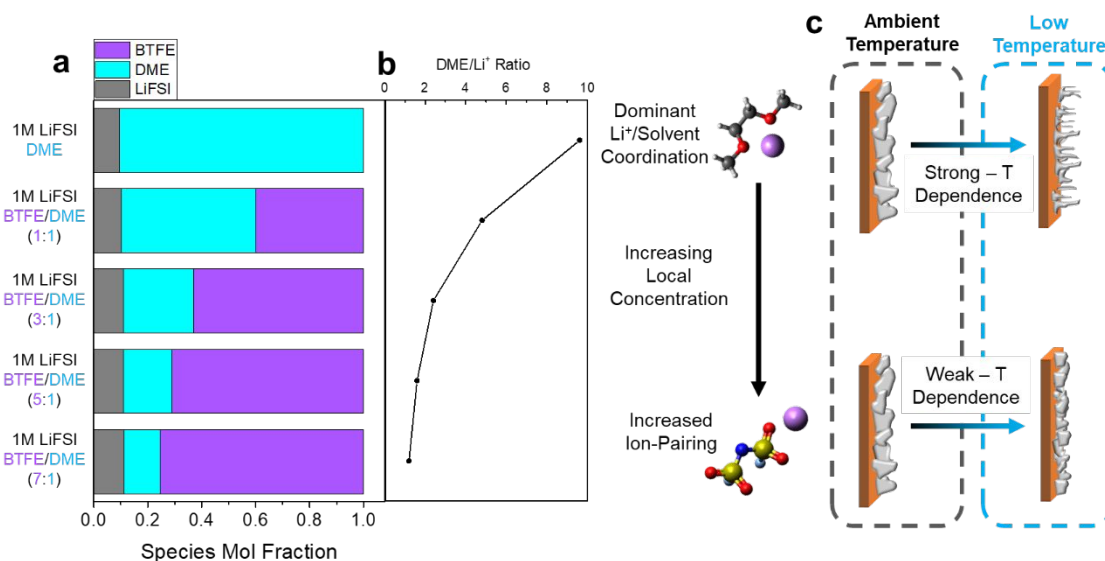101 capable of charging *and* discharging at low temperatures, as illustrated in Figure 1.

Figure 1. Overview of **a)** electrolytes of interest and their molar composition, **b)** coincident effect of molar DME/Li$^+$ ratio on ion-pairing in solution, and **c)** the effect of these factors on the temperature dependence of Li cycling.

102

103   To provide a basis for the assessment of low temperature Li metal performance and the

104 eventual design of LMB full batteries, physical characterization of the DME-based electrolytes of

105 interest was first conducted. Though our previous results have indicated exceptional ionic

106 conductivity is not necessarily a prerequisite for reversible low temperature Li metal

107 performance[23], the freezing of electrolytes and exponential increases in their viscosity is known

108 to overwhelm electrochemical performance.[11,21] As shown in Figure 2a, it was confirmed that all

109 systems of interest remained in a liquid state down to -60 °C. To provide an insight into the effect

110 of temperature on ionic transport, the ionic conductivities were also measured (Figure 2b). It was

111 found that the systems of lowest local concentration (i.e., lowest DME/LiFSI ratio but still 1 M

112 with respect to the total volume of BTFE and DME) displayed far superior transport, where the 1

113 M LiFSI in DME, 1:1, 3:1, 5:1, and 7:1 BTFE/DME electrolytes displayed ionic conductivities of

114 15.2, 11.2, 9.18, 3.60, and 2.43 mS cm^{-1} at 20 °C, respectively. This trend was largely maintained

115 at low temperature, where the systems retained 6.20, 2.87, 2.54, 0.87, and 0.50 mS cm^{-1} at -40 °C,

116 respectively. The reduction of bulk conductivity with increased ion-pairing is well-established,

117 and can be generally described by a reduction in ionicity due to the strong interactions between

118 cation and anion.[28,33] It is also noteworthy that the inclusion of BTFE in the electrolytes were

119 found to slightly increase the viscosity, where the 1 M LiFSI DME, 1 M LiFSI BTFE/DME (1:1)

120   and 1 M LiFSI BTFE/DME (5:1) electrolytes displayed viscosities of 1.7, 2.7, and 2.4 cP,

121   respectively, however the viscosity of these systems all remains below that of conventional

122   carbonate systems (Figure S1). Although ion-pairing is hypothesized to result in improved charge-

123   transfer kinetics, its tradeoff with bulk transport may indicate that an intermediate concentration

124   may be optimal for low-temperature LMB applications.

125   Electrolytes utilizing DME generally display poor oxidative stability due to the inherent

126   HOMO energy of ether solvents.[29,34,35] Though these systems are typically applied in Li-S

127   batteries, the low-temperature performance degradation of the S cathode has been observed to be

128   severe, due in large part to clustering processes inherent to the polysulfide conversion process.[1]

129   As such, transition metal oxide cathode hosts remain to be highly desirable for low temperature

130   applications, which require the oxidative stability of the electrolyte to exceed 4 V vs. Li/Li$^+$.

131   Despite its disadvantages for ion transport through the bulk, increased local concentration (and

132   increased ion-pairing) is known to produce advantageous effects on the electrochemical stability

133   of the system.[25-29] This was found to be the case for the DME-based LHCE systems investigated

134   here as well, where the areal current produced by linear-scan voltammetry (LSV) on an Al current

135   collector was found to exceed 0.02 mA cm^{-2} at 4.22, 4.31, 5.34, > 5.5, and > 5.5 V for 1 M LiFSI

136   in DME, 1:1, 3:1, 5:1, and 7:1 BTFE/DME, respectively (Figure 2c). However, it is worth noting

137   that there is a slight increase in oxidative current between 3.7 and 4.5 V within the 3:1 LSV profile,

138   which indicates that a slight decomposition reaction occurs to form a passivating interphase, after

139   which the current decreases again. It was also found that these trends were maintained in the

140   presence of conductive carbon and NMC 811, where 1 M LiFSI DME and 1 M LiFSI BTFE/DME

141   (1:1) showed significantly increased decomposition behavior at lower voltages than their

142   counterparts (Figure S2).

143   The transport and electrochemical stability trends are a direct symptom of increased ion-

144   pairing due to heightened local concentrations (i.e., lower DME/Li$^+$ ratio). To observe this

145   experimentally and to serve as an aid to future computational studies, Raman spectroscopy was

146   carried out on the electrolytes of interest and their pure components (Figure 2d). It was found that

147   the S-N-S bending peak of the FSI$^-$, present in the salt spectra at 774 cm^{-1}, undergoes a significant

148   shift to 719 cm^{-1} when dissolved at 1 M in DME, indicative of the separation between Li$^+$ and FSI$^-$

149   produced by the DME. This peak was then found to progressively shift to 732 cm^{-1} in the 3:1

150 mixture, which indicates an increase in ion-paring between Li^+ and FSI^- in solution.[28] Though the

151 peak shift between 1 M LiFSI DME and 1 M LiFSI BTFE/DME (3:1) appears to be linear, it is

152 noteworthy that this shift is substantially heightened between the 3:1 and 5:1 systems.

153 Additionally, the 5:1 and 7:1 mixtures display much broader S-N-S peaks, indicating an increased

154 amount of bound FSI^- solvation states within the system. Moreover, a similarly large reduction in

155 conductivity was observed between the 3:1 and 5:1 mixtures (Figure 2b). This ion-pairing was also

156 found to result in a slight but incremental increase in Li^+ transference number, from 0.32 in 1 M

157 LiFSI DME to 0.53 in the 7:1 system (Figure S3). Though this increase is significant, our previous

158 work indicates that such an increase has little effect on the interphasial Li^+ depletion when

159 observed in tandem with a reduction of ionic conductivity of such a magnitude.[23] These

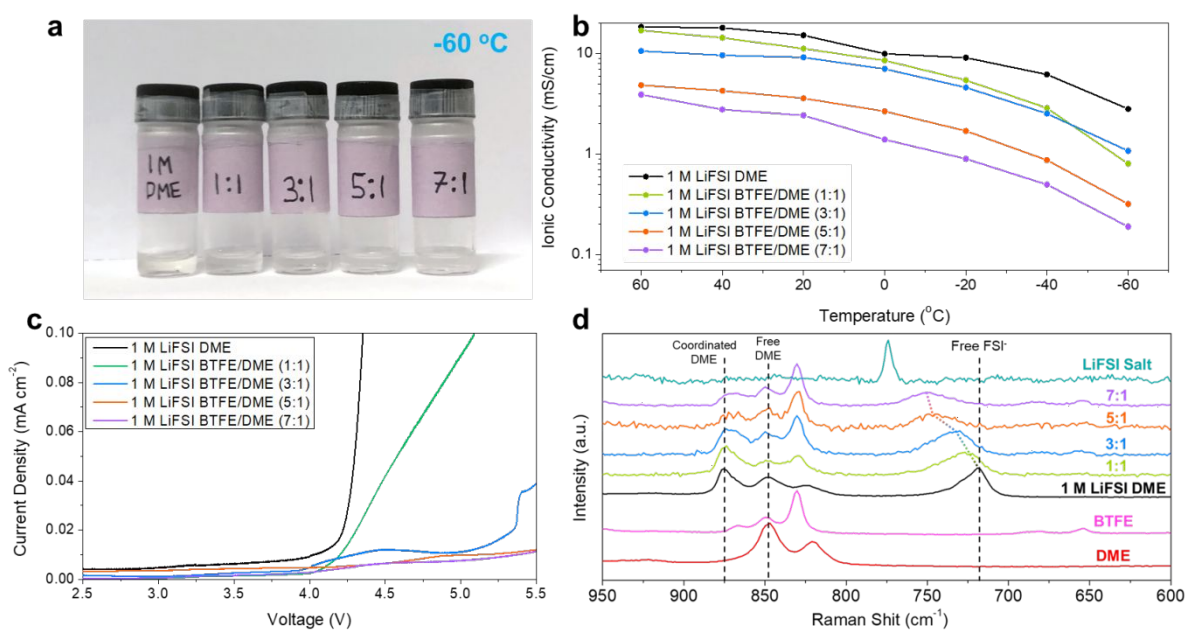160 phenomena are further examined in the molecular dynamics analysis below.

Figure 2. Physical and electrochemical properties of the electrolytes of interest. **a)** Optical photograph of electrolytes at -60 °C. **b)** Measured ionic conductivity across temperature. **c)** Oxidative linear scan voltammetry of selected systems on Al current collectors at 1 mV s^{-1}. **d)** Raman spectra of the electrolytes and their pure

161

162 To examine the implications of these electrolyte properties on low-temperature LMB

163 reversibility, the CE of Li plating was determined in Li||Cu cells via the accurate galvanostatic

164 method proposed by Adams *et al*.[36] Testing at 23 and -20 °C was conducted at 0.5 mA cm^{-2}

165 whereas we used 0.25 mA cm^{-2} for -40 and -60 °C. Due to the intrinsic reductive stability of ether

166 solvents and the fluorine-donating capabilities of LiFSI, 1 M LiFSI DME, and 1 M LiFSI 1:1, 3:1,

167　5:1, and 7:1 BTFE/DME systems were found to display reversible CEs of 96.0, 99.1, 99.1, 99.4,

168　and 99.4% at room temperature (Figure 3a). These CEs were also found to persist over many

169　plating and stripping cycles (Figure S4). The relatively improved CEs of the electrolytes

170　containing BTFE is likely due to the increased prevalence of fluorine in the SEI layers, which was

171　confirmed via XPS (Figure S5), however the chemical identity of the SEI was found to be

172　relatively similar across systems, which agrees with previous literature.[37] However, when the

173　temperature was reduced it was found that the scaling of such reversibility was not equal across

174　the systems. In particular, systems of lower local concentration displayed substantial noise in the

175　voltage curves, which can be attributed to soft-shorting events at low temperature and contribute

176　to extremely reduced CEs.[9,23] Specifically, the 1 M LiFSI DME electrolyte was found to short at

177　-20 $^{\circ}$C, whereas the CE of the 1:1 mixture reduced to 94.8% at -20 $^{\circ}$C (Figure 3b), before finally

178　shorting at -40 $^{\circ}$C. At -40 and -60 $^{\circ}$C, the 3:1, 5:1, and 7:1 electrolytes were found to produce

179　reversible CEs of 98.9, 98.5, 98.6, and 96.6, 96.9, 96.4 %, respectively (Figure 3c,d). A summary

180　of these trends is shown in Figure 3e for ease of comparison.

181　　　Additionally, the critical current for each electrolyte was assessed in Li‖Li cells at each

182　temperature. The profiles for these tests are shown in Figure S6, where it was found that the 1 M

183　LiFSI BTFE/DME (5:1) electrolyte maintains critical currents of 5, 3, and 0.75 mA cm^{-2} at -20, -

184　40, and -60 $^{\circ}$C, which is the highest among the investigated systems. It is also worth noting that

185　the critical current often exceeds the shorting currents observed in Li‖Cu tests, which implies that

186　nucleation of Li on Cu also plays a role in the poor performance. Indeed, previous reports have

187　observed a substantial variance in nucleation behavior at reduced temperatures.[31] A summary of

188　these critical currents is shown in Figure 2f, which provides a basis for safety assessment at the

189　full cell level. Crucially, we note that the optimal electrolytes for low temperature Li metal

190　performance and ionic conductivity do not align, which agrees with previous reports and indicates

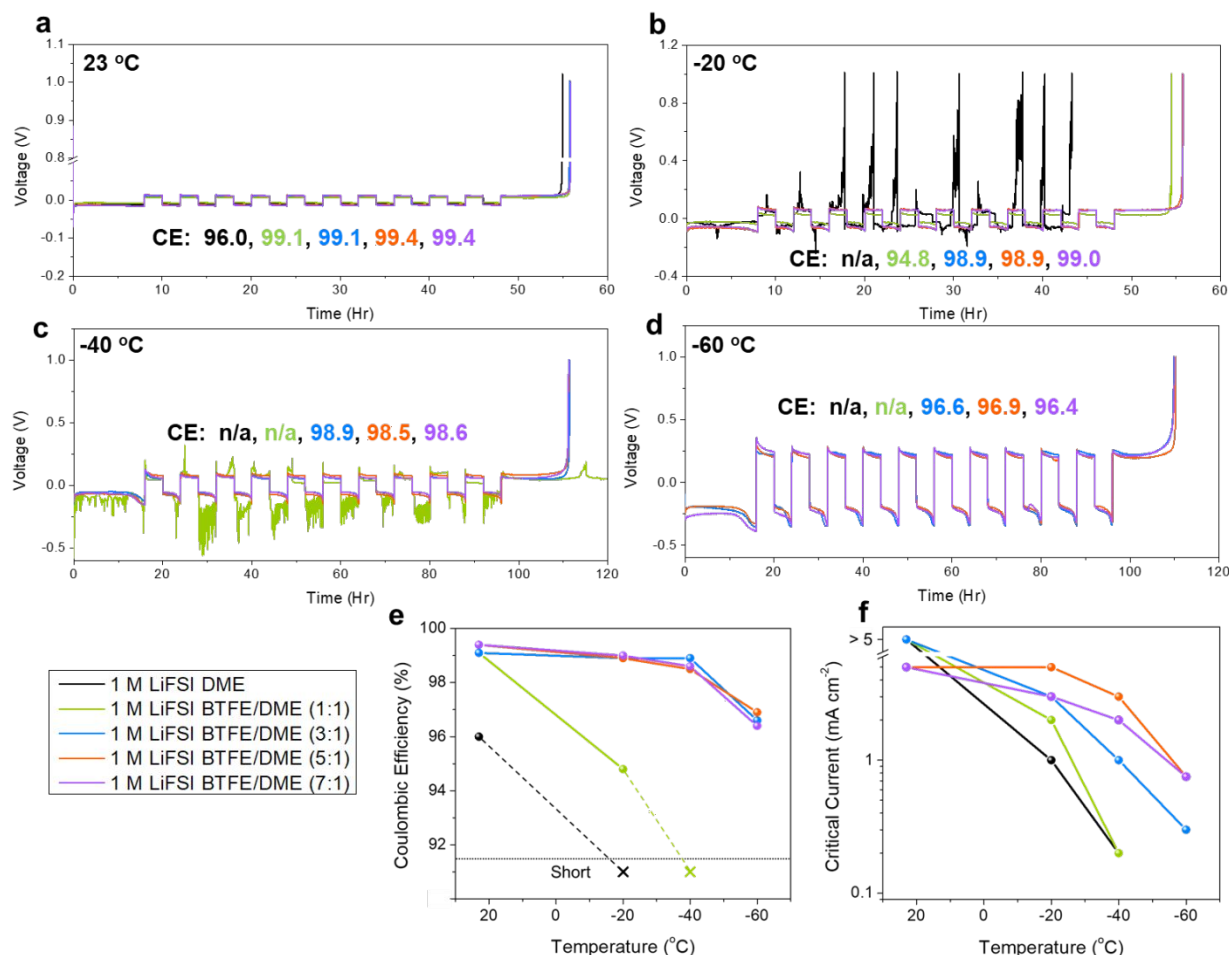191　that the low temperature performance is dictated by charge-transfer.[22,23]

192

Figure 3. Li metal performance measurements at room and low temperature. Voltage profiles of Li/Cu cells employing electrolytes of interest at **a)** 23 °C and 0.5 mA cm^{-2}, **b)** -20 °C and 0.5 mA cm^{-2}, **c)** -40 °C and 0.25 mA cm^{-2}, **d)** -60 °C and 0.25 mA cm^{-2}. In all cases a conditioning cycle was conducted and not shown. Summaries of **e)** Coulombic efficiency and **f)** Critical current of the electrolytes of interest at various temperatures.

193

194   To further understand the interplay between ion-pairing and Li metal performance at low

195   temperature from a morphological standpoint, scanning electron microscopy (SEM) was

196   conducted on Li deposited on Cu current collectors at 23 and -40 °C. Photographs taken of the Cu

197   electrodes after deposition at 23 °C reveal metallic Li deposits with a silver appearance, which is

198   typically indicative of micron-scale Li deposits, as uncontrolled nanoscale morphologies typically

199   appear black in color (Figure 4a). SEM images of the Li deposited at room temperature confirm

200   this, where Li was found to deposit in the "chunk" morphology often associated with electrolytes

201   of similar composition.[28-30,37] Interestingly, the micro-scale uniformity was found to increase

202   coincidently with increasing local concentration. This may be a direct result of the increased

203   electrochemical stability of the electrolyte associated with higher concentration, where salt driven

204 passivation of the interphase is typically achieved due to the restriction of reactive solvent by the

205 strongly coordinated Li$^+$.[25-29,33-35,37]

206   When carrying out the same deposition process at -40 °C we observed a distinct shift in

207 both the macroscopic and microscopic structure, however. Similar to the previously presented data,

208 we believe the origin of this behavior and its asymmetric temperature dependence across systems

209 corresponds to the local concentration of each system and the coincident ion-pairing of their

210 solvation shells. First, it was observed that the amount of Li plated on the Cu current collectors in

211 1 M LiFSI DME and 1 M LiFSI BTFE/DME (1:1) undergoes a severe reduction at -40 °C. This

212 phenomenon has been observed in our previous work[23] and is believed to be a direct indication

213 that these systems suffer from severe shorting at low temperature which renders Li plating

214 unnecessary to balance the charge of the electrochemical circuit. Furthermore, bundles of nano-

215 sized dendritic filaments were observed in the 1 M LiFSI DME sample (Figure S7), which may be

216 directly responsible for the shorting behavior. On the other hand, homogenous Li deposition was

217 achieved in 1 M LiFSI BTFE/DME 3:1, 5:1, and 7:1 systems, which agrees with the trends

218 observed in the CE measurements at -40 °C and below. Notably, the optimum in terms of deposit

219 size and uniformity at -40 °C was produced by 1 M LiFSI BTFE/DME (5:1) instead of the 7:1

220 solution, which may suggest that among systems of comparable charge-transfer kinetics the

221 relatively poor ionic conductivity of the 7:1 electrolyte may be problematic. Despite this, the

222 reduced Li deposition size produced by the 7:1 electrolyte at -40 °C did not result in a clear

223 reduction in CE relative to the 3:1 and 5:1 electrolytes, which is likely related to the inherently

224 lower reactivity of this heavily ion-paired system. We have also observed dendritic growth in the

225 Li deposits produced by 1 M LiFSI BTFE/DME (1:1) at -20 °C, which coincides with a substantial

226 decrease in CE despite the lack of soft-shorting phenomena (Figure S8). Such dendritic growth

227 was also found to result in a significant increase in plated Li porosity, where 4 mAh cm^{-2} of plated

228 Li was found to exhibit thicknesses of 32.7, 25.3, 22.6, and 23.2 μm for 1 M LiFSI BTFE/DME

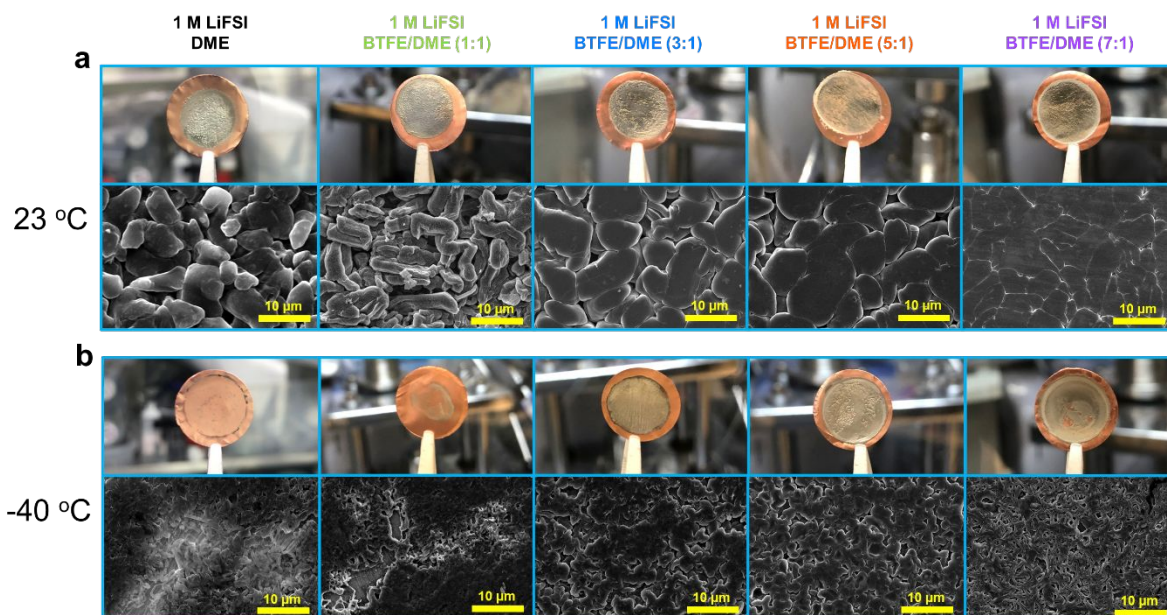229 (1:1), (3:1), (5:1), and (7:1), respectively (Figure S9).

Figure 4. Characterization of Li metal deposits in electrolytes of interest. Optical and SEM photographs of 5 mAh cm^{-2} of Li metal deposited at **a)** 23 °C and **b)** -40 °C. All depositions were carried out at 0.5 mA cm^{-2}.

230

231   As previously discussed, the charge-transfer barrier is thought to be the limiting factor at
232   low temperatures. Such behavior and its temperature dependence is defined by the inner and outer-
233   sphere reorganization energies (further discussed below), themselves defined by the solvation
234   environment of Li$^+$ in solution.[22,38-42] To understand this microscopic solvation structure in the
235   LHCE systems, we performed classical MD simulations. Here, ~ 500 total molecules were
236   assembled in various ratios of Li$^+$, FSI$^-$, DME, and BTFE, depending on the electrolyte in question
237   (Table S1), and subjected to 25 ns of production dynamics after initial equilibration, from which
238   the solvation data were extracted. A more detailed description of these simulations is provided in
239   the Supporting Information. Representative snapshots from the MD simulations can be found in
240   Figure 5a, where it can be seen that the spatial distribution of the ions shift substantially as the
241   concentration increases. At the highest DME/Li$^+$ ratio (9.6:1) found in 1 M LiFSI DME, the Li$^+$
242   ions are distributed homogenously in solution. However, at the higher local concentrations found
243   in the 3:1 electrolyte and above, significant aggregation of solvating clusters composed of Li$^+$, FSI$^-$
244   and DME separated by regions of BTFE was found. This local aggregation effect is also observed
245   in a previous ab-initio MD work[43], and partially accounts for the reduced ionic conductivity of
246   the systems with high local concentrations. The stochastic trajectory of the Li$^+$ ion over the 25 ns
247   is presented in Figure S11 to visualize the effect of aggregation on ionic motion. We reason that

248   this effect is a symptom of the disparate solvating power of DME and BTFE, where the Li$^+$ ion far

249   prefers interaction with the former, forming ion-pairs as the amount of available DME

250   decreases.[28]

251   To quantify the local environment around the Li$^+$ ion in solution, the radial distribution

252   function (RDF) with respect to Li$^+$ was calculated. Figure 5b,c shows the RDF due to the oxygens

253   of DME and FSI$^-$ respectively, and the associated integrals (i.e. the coordination number) is shown

254   in Figure 5d and e. This analysis revealed that 1 M LiFSI in DME largely prefers a solvent-

255   separated ion-pair structure (SSIP), in which the Li$^+$ is coordinated only by solvent in the first

256   solvation shell. Our previous work has noted that the DME dominated SSIP solvation environment

257   is correlated with poor low temperature performance.[23] However, with increasing local

258   concentration (increased BTFE/DME ratio) the DME in the primary solvation shell was

259   sequentially displaced by FSI$^-$ molecules, such that the average coordination of environments of

260   the 1 M LiFSI DME and 7:1 electrolytes were calculated to be Li$^+$(DME-O)$_{5.0}$(FSI-O)$_{0.3}$ and

261   Li$^+$(DME-O)$_{3.0}$(FSI-O)$_{2.5}$, respectively. BTFE was not found to solvate Li$^+$ in any statistically

262   significant manner (Figure S12), which is also supported by the Raman spectra (Figure 2d). It is

263   noteworthy that there is generally a distinction made between different ion-paired states, where

264   one coordinating FSI$^-$ per Li$^+$ is typically deemed a "contact-ion-pair" (CIP), while FSI$^-$

265   coordination numbers > 1 are denoted as an "aggregate" (AGG).[26] In this regard, the RDF data

266   suggests that SSIP, CIP, and AGG structures dominate as the local concentrations increases.

267   Though the RDF data reveals the *average solvation structure*, in this case, they fail to

268   properly describe the *distribution* of solvation states the Li$^+$ takes in each system. To explore this,

269   250 snapshots of each Li$^+$ and its local environment were extracted for each simulation (between

270   10,750 and 12,500 snapshots depending on the simulation) and tabulated (Supporting

271   Information). In this analysis, we adopted the naming convention "X-Y-Z" to denote the number

272   of DME (X), FSI$^-$ (Y), and BTFE (Z) found within the first solvation shell of Li (within 3 Å). It

273   was found that the 1 M LiFSI DME electrolyte most prominently displayed a local environment

274   of 3-0-0 (68.5 %), with a lower prevalence of 2-1-0 (27.8 %) which correspond to SSIP and

275   contact-ion-pair (CIP) solvation environments, respectively. More moderate local concentrations

276   (e.g., 3:1) were found to be dominated by CIP, while the higher concentrations tended to prefer

277   AGG states. Though the calculated Li$^+$ transference numbers indicate that the MD simulations

278   may slightly exaggerate the ion-pairing character of these systems, this trend is maintained (Figure

279   S3). Representative structures for each system are shown in Figure 2f, and alternatively displayed

280   in Figure S12f. Consistent with our previous work,[23] we now elaborate on how the CIP/aggregate

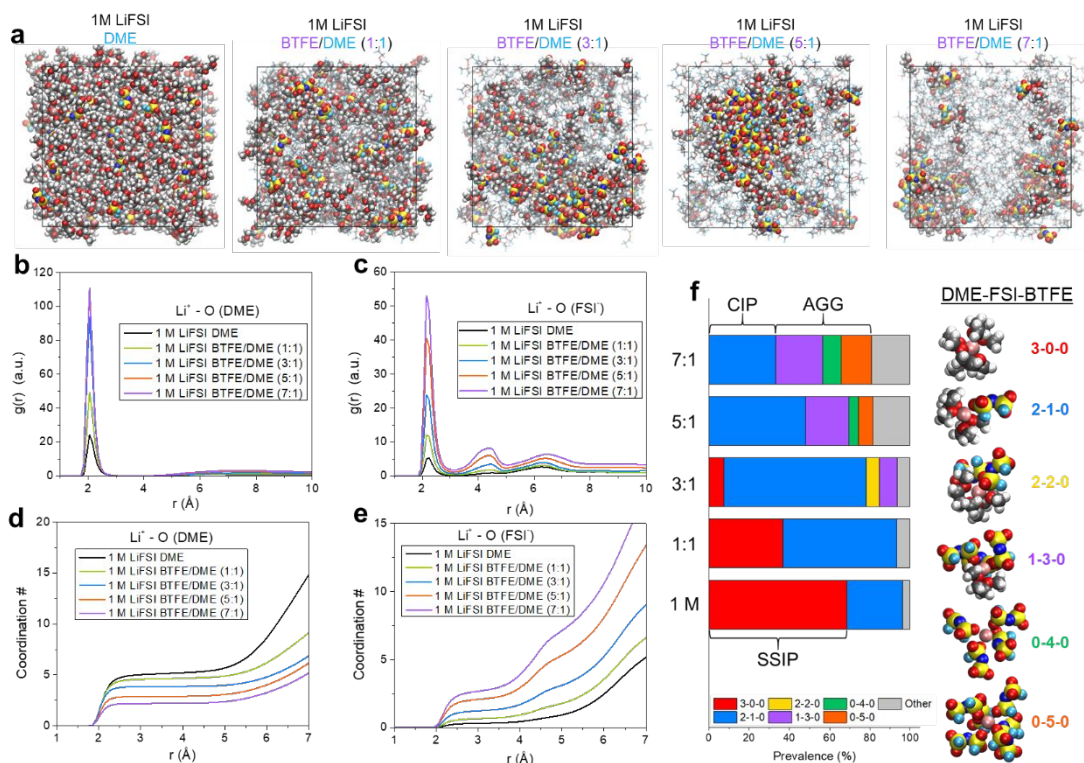281   dominated systems are advantageous at low temperatures.

282

Figure 5. Molecular dynamics analysis of electrolytes of interest. **a)** Snapshots of MD simulations. Radial distribution functions of **b)** DME and **c)** FSI$^-$ oxygens with respect to Li$^+$. Coordination numbers of **d)** DME and **e)** FSI$^-$ oxygens with respect to Li$^+$. **f)** Solvation structure distribution analysis of systems of interest and representative MD snapshot of each significant coordination environment.

283

284   It has been widely observed that charge transfer impedance at low temperatures

285   overwhelms and thus dictates the performance of Li-based batteries at low temperatures, which

286   we have recently hypothesized to be the cause of the dendritic growth and subsequent shorting of

287   LMBs under such conditions.[2,22,23] The experimental and theoretical evidence presented in this

288   work establishes a more robust correlation between ion-pairing and improved Li reversibility at

289   low temperature. While this information is practically useful for low temperature electrolyte

290   design, it is crucial to note that a causal string has not yet been identified. The temperature

291   dependence of charge-transfer in Li-based batteries is a complicated topic that undoubtedly

292   warrants further study, however there are a number of recent works that may provide additional

293   insights into the phenomena observed here.

294   To gain further insights into the charge-transfer phenomena, we take a perspective based

295   on Marcus Theory. This framework and its subsequent iterations are generally thought to be the

296   most accurate model of electrochemical kinetics at the interphase, and have recently been

297   demonstrated to accurately describe Li metal plating.[38-42,44] Perhaps the most relevant parameter

298   to our work, which partially defines both the adiabaticity and energy of the transition state is the

299   reorganization parameter λ, which generally consists of inner-sphere and outer-sphere

300   components. The former describes the reorganization energy of the electronic structure and

301   vibrational modes within the solvation sphere, while the latter describes the energetic cost of

302   nuclear motion (i.e., deformation) of the coordinating species. To interpret the results presented

303   here, and in keeping with previous studies[39-41], it is generally assumed that inner-sphere

304   reorganization is largely temperature *independent*, whereas outer-sphere reorganization is

305   significantly temperature *dependent*.

306   The effect of ion-pairing on these reorganization factors has been typically studied in a

307   variety of electrochemical systems, where it has been suggested that increased pairing results in

308   improved outer-sphere energetics.[45,46] In aprotic media, the formation of ion-pairs in the double

309   layer has been proposed to allow the cation to approach the interphase at smaller distances than

310   SSIP structures[46], which preliminary quantum chemistry results indicate may be the case in this

311   work, where FSI⁻ removal was found to be unlikely when compared to DME removal (Figure S13).

312   It is also worth noting that different degrees of ion pairing were found to display different behavior

313   at said interphases, which may also describe the variance in performance between the 3:1, 5:1, and

314   7:1 electrolytes.[46] However, recent work from Boyle et al. indicates that these conclusions may

315   not directly translate to improved Li metal kinetics at room temperature.[44] This work found that

316   though the interphasial impedance was substantially lowered by the introduction of ion-pairs, the

317   reorganization parameter underwent little change. We hypothesize that this is a direct result of an

318   increased contribution from e⁻ transfer resistance (i.e. inner-sphere) to the total reorganization

319   energy in ion-paired systems. Additionally, the presence of ion-pairing was also concluded to

320   reduce the electronic coupling between the electrode and Li⁺, which may be a direct result of

321   increased binding energy between Li⁺ and the anion (Figure S13). While this reduced coupling is

322   broadly detrimental to charge-transfer, the nature of electronic phenomena suggests it has little

323   influence on temperature dependent performance. Considering the temperature dependence of

324   inner and outer-sphere reorganization, these results would predict that the increased ion pairing in

325   our systems gives rise to similar behavior at room temperature, but leads to disparate scaling at

326   low temperatures, consistent with our experimental findings. Further, our model is supported by

327   the recent work from Wang et al., which suggested that electrolytes dominated by Li^+/DME

328   interactions have a particularly large entropy of Li/Li^+ exchange, which is incrementally reduced

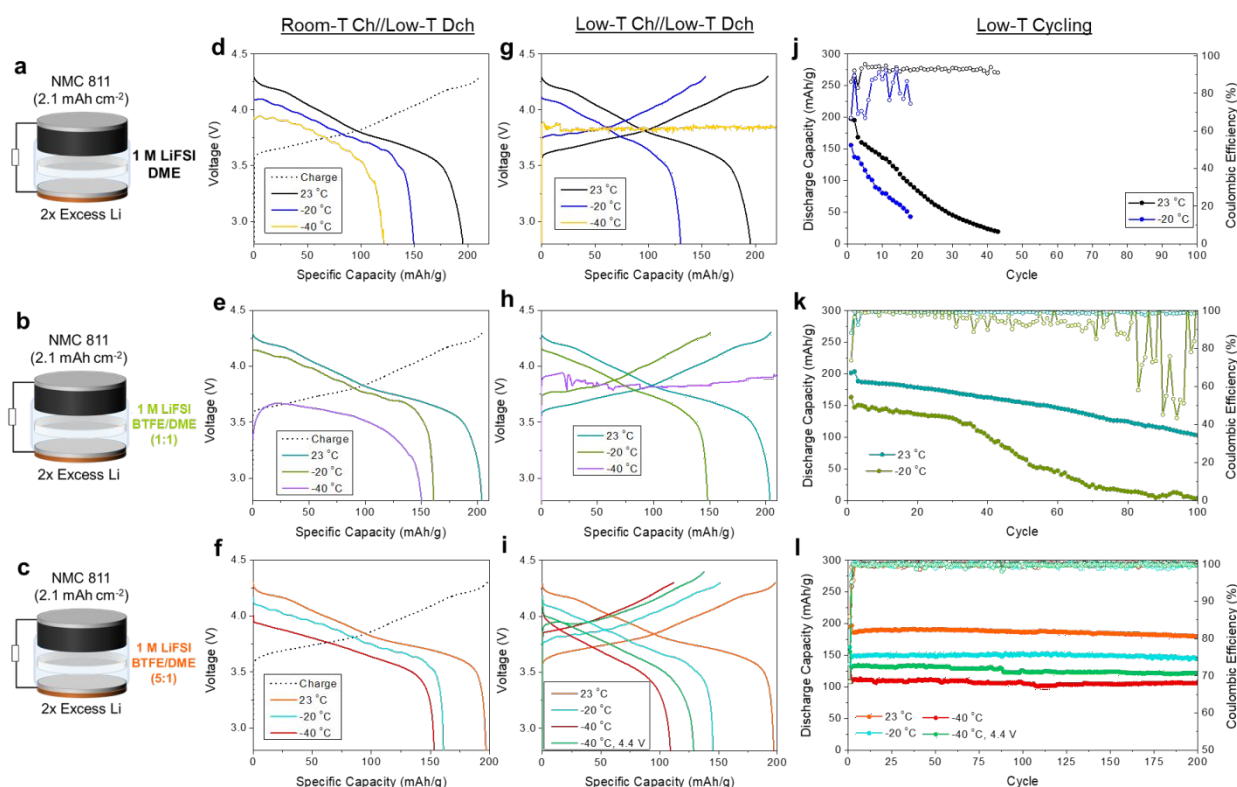329   by the introduction of ion-pairing in solution.[32]

Figure 6. 2x Li‖NMC 811 full cell operation at room and low temperature. Schematics of full cells employing **a)** 1 M LiFSI DME, **b)** 1 M LiFSI BTFE/DME (1:1), and **c)** 1 M LiFSI BTFE/DME (5:1) under flooded electrolyte conditions. 0.1 C rate discharge profiles of full cells charged at room temperature employing **d)** 1 M LiFSI DME, **e)** 1 M LiFSI BTFE/DME (1:1), and **f)** 1 M LiFSI BTFE/DME (5:1). Cycle profiles of full cells charged and discharged at various temperatures employing **g)** 1 M LiFSI DME, **h)** 1 M LiFSI BTFE/DME (1:1), and **i)** 1 M LiFSI BTFE/DME (5:1). All displayed voltage profiles represent the first available cycle post conditioning step. Cycling performance of full cells employing **j)** 1 M LiFSI DME, **k)** 1 M LiFSI BTFE/DME (1:1), and **l)** 1 M LiFSI BTFE/DME (5:1). Room temperature cycling was carried out at C/3‖C/3 rates after 2 cycles at C/10 and low temperature cycling was carried out at C/10‖C/5 for charge‖discharge, respectively. Full cells were charged once at room temperature before transferring to low temperature.

330

331   Though a definitive causal understanding of temperature dependent Li metal plating has

332   not been reached, this work demonstrates that the introduction of ion-pairing in the electrolyte

333   results in vastly improved Li metal cycling at low temperatures. To provide a more practical

334   demonstration of these advantages, 2x excess Li||NMC 811 full cells were assembled and subjected

335   to a variety of performance tests at room and low temperatures. The 1 M LiFSI DME and 1 M

336   LiFSI BTFE/DME (1:1) systems were applied as SSIP-containing controls and compared to 1 M

337   LiFSI BTFE/DME (5:1) due to its relative balance between low temperature CE, critical current,

338   and oxidative stability (Figure 6a,b). Though the systems exhibiting an SSIP structure are sub-

339   optimal choices due to their reduced oxidative stability (Figure 2c, S2), such a comparison is

340   necessary to examine the influence of solvation structure on low temperature energy retention and

341   cyclability. These cells were assessed in two modes of operation: charging at room temperature

342   followed by a low temperature discharge, and both charging *and* discharging at the temperature of

343   interest. As shown in Figure 6d and 6e, the cells employing 1 M LiFSI DME and 1 M LiFSI

344   BTFE/DME (1:1) were found to output 195, 149, and 122 mAh g^{-1} and 203, 163, and 154 mAh g^{-1}

345   (with respect to the cathode), respectfully when discharged at 23, -20, and -40 °C and after being

346   charged at room temperature. The relative increase in low temperature discharge capacity between

347   1 M LiFSI DME and the 1 M LiFSI BTFE/DME (1:1) system is possibly due to the increased CIP

348   character in the 1:1 mixture. Conversely, the 1 M LiFSI BTFE/DME (5:1) full cells displayed 197,

349   161, and 153 mAh g^{-1} under the same conditions, indicative of improved electrochemical kinetics

350   over the controls despite significantly reduced bulk transport metrics (Figure 6f). Note that this

351   operation scheme does not involve Li plating at low temperature and thus shorting was

352   intentionally avoided.

353   High performance retention in the 5:1 electrolyte was also observed when subject to both

354   charge *and* discharge at reduced temperature, displaying discharge capacities of 145 and 109 mAh

355   g^{-1} at -20 and -40 °C, respectively (Figure 6i). It is noteworthy that the ohmic polarization of

356   discharge at -40 °C is slightly improved compared to that which was charged at room temperature

357   (Figure 6f), which may be due to the higher surface are of Li, or variance of the SEI formed at

358   such temperatures.[9] Additionally, it was found that this output capacity could be increased to 129

359   mAh g^{-1} by increasing the cutoff voltage from 4.3 V to 4.4 V at -40 °C, which may partially

360   compensate for ohmic losses on the anode side at low temperature. This performance is not shared

361   by the 1 M LiFSI DME and 1 M LiFSI BTFE/DME (1:1) electrolyte cells under the same

362   conditions, which retained 130 and 147 mAh g^{-1} when charged and discharged at -20 °C before

363   undergoing complete soft shorting at -40 °C. As previously discussed, we attribute these results to

364   the favorable temperature scaling of the charge-transfer process in ion-paired electrolytes, which

365   is consistent with 3-electrode impedance studies, which show a substantially reduced barrier for

366   the 5:1 electrolyte down to -40 °C for both the cathode and anode (Figure S14).These performance

367   results are consistent with the critical current results, and demonstrates that electrolytes which

368   exhibit SSIP structures are untenable for application in low temperature LMBs.

369   When subjected to cycling, the 1 M LiFSI DME full cells were found to be unable to retain

370   meaningful capacity, retaining 136 and 80 mAh g^{-1} after 10 cycles at 23 and -20 °C, respectively

371   (Figure 6j). This performance is likely a combined effect of the poor oxidative stability of the

372   electrolyte, which may exacerbate transition metal dissolution on the cathode side, as well as the

373   comparatively poor Li reversibility of the 1 M LiFSI DME system.[47] Full cells employing the 1:1

374   electrolyte retained 154 and 103 mAh g $^{-1}$ after 50 and 100 cycles at 23 °C, representing a

375   substantial improvement over the 1 M LiFSI DME electrolyte, which may be partially due to the

376   stability of the cathode electrolyte interphase (CEI) formed by BTFE (Figure S15). Hence, the 1

377   M LiFSI BTFE/DME (1:1) and provides a valid cycling baseline at ambient temperature to

378   examine the effect of solvation structure on low temperature performance. As predicted by the

379   previous trends (Figure 3), the poor Li metal cycling efficiency of the 1:1 electrolyte at -20 °C

380   (Figure 3b) was found to severely limit performance, where the output capacity significantly

381   decreased after 30 cycles, falling to 66 and 3.7 mAh g^{-1} at the 50th and 100th cycle, respectively

382   (Figure 6k). On the other hand, the full cells employing 1 M LiFSI BTFE/DME (5:1) were found

383   to retain stable performance over 200 cycles without undergoing a meaningful reduction in output

384   capacity or coulombic efficiency that is generally associated with exhaustion of the Li metal anode

385   reservoir (Figure 6l).[30] The capacity retention of these cells after 100 cycles were found to be

386   187, 153, 108, and mAh g^{-1} at 23, -20, -40 (4.3 V cutoff), and -40 °C (4.4 V cutoff).The improved

387   performance of the 1 M LiFSI BTFE/DME (5:1) electrolyte is evidence that LMBs can be cycled

388   at low temperature reversibly without the need for thermal management.

389   To supplement the performance assessment of coin cells employing the electrolytes of

390   interest, scale-up projections were carried out to provide the expected energy density as a function

391 of temperature and operating scheme. The projections were based on 5 Ah pouch cells at an N/P

392 capacity ratio of 2 (2x excess Li) and a 3 g Ah^{-1} electrolyte loading, with the specific capacities

393 and average voltages taken from the first cycle of the coin cell data (Figure S16). More details are

394 available in the Supporting Information. At a cathode loading of 2 mAh cm^{-2}, these projections

395 estimate that pouch cells employing 1 M LiFSI DME and charged at room temperature could

396 achieve energy densities of 303, 237, and 192 Wh kg^{-1} whereas cells employing 1 M LiFSI

397 BTFE/DME (1:1) project to produce 309, 247, and 213 Wh kg^{-1} at 23, -20, and -40 °C, respectively.

398 Under the same conditions, the 1 M LiFSI BTFE/DME (5:1) is expected to achieve 307, 250, and

399 230 Wh kg^{-1}. When both charged *and* discharged at the temperature of interest, the 1 M LiFSI

400 DME energy densities are expected to fall to 207, and 0 Wh kg^{-1} (due to shorting) whereas 1 M

401 LiFSI BTFE/DME (1:1) are expected to fall to 226, and 0 Wh kg^{-1} at -20 and -40 °C, respectively.

402 Conversely, the 5:1 electrolyte is expected to output 224, 163, and 194 Wh kg^{-1} at -20, -40 (4.3 V

403 cutoff), and -40 °C (4.4 V cutoff), respectively. Additionally, increasing the cathode loading to 3

404 mAh cm^{-2} in the 5:1 electrolyte under the same conditions is expected to increase these values to

405 342, 249, 181, and 216 Wh kg^{-1} at 23, -20, -40 (4.3 V cutoff), and -40 °C (4.4 V cutoff),

406 respectively. Preliminary results indicate this optimization may be possible (Figure S17), however

407 the engineering of practical LMB pouch cells capable of low temperature cycling remains a

408 difficult task. If such a battery were realized at scale, the NASA 20LuSTR program goals of a >

409 250 Wh kg^{-1} secondary battery operating at < -40 °C for over 100 cycles would be within reach.[48]

410 While the electrolytes investigated here provide a scientific comparison of the effects of ion-

411 pairing on the temperature dependence of Li metal reversibility, it should be noted that electrolytes

412 employing solvents of a lower Li^+ binding energy may improve the performance even further at

413 low temperatures.

414

Conclusions

416   A series of LHCE electrolytes composed of LiFSI, DME, and BFTE with varying local

417 concentrations were designed and compared to probe the effect of ion-paring in the local solvation

418 structure on the low temperature performance of Li metal plating and stripping. It was found that

419 despite comparable room temperature performance, only systems with DME/Li^+ molecular ratios

420   of 2.4 and below were capable of providing reversible Li cycling at -20 $^{\circ}$C and below. What's

421   more, this performance trend was found to be in opposition to the ionic transport data, which

422   seemed to indicate that systems of low local concentration were superior. Through MD analysis,

423   it was found that this performance transition was coincident with a distinct shift in Li$^+$ solvation

424   structure in which ion-pairing was a defining feature, and purely solvent dominated environments

425   were due to the lack of available DME molecules. Though this evidence is still correlational in

426   nature, previous reports indicate that ion-pairing may shift the balance of inner-sphere, which is

427   thought to be temperature independent, and outer-sphere reorganization energies such that low-

428   temperature performance is improved. Finally, 2x excess Li||NMC 811 full cells were assembled

429   utilizing both electrolytes of high and low local concentrations to demonstrate the translation of

430   these solvation effects during cell operation. Specifically, the cells employing electrolytes with

431   significant ion-pairing nature were able to demonstrate 100 cycles of reversible performance with

432   little capacity fade while retaining 63 % of their room temperature energy. This work

433   unambiguously demonstrates the positive effects of ion-paired solvation structures on the low

434   temperature Li metal reversibility while providing a viable route to LMBs charged *and* discharged

435   at low temperatures.

Acknowledgements

Author Contributions

451   J.H. conceived the original idea. P.L. and Z.C. directed the project. J.H., and K.K., carried out the
452   experiments. Y.Y., Z.W., H.L., and M.L. assisted with characterization. T.A.P directed the
453   computational experiments. J.H. and A.C. conducted computational experiments. H.G. and G.C.

454 assisted in experimental design and data processing. J.H., Z.C., P.L., and T.A.P wrote the paper.
455 All authors discussed the results and commented on the manuscript.

456

457 **Competing Interests**

458 The authors declare no competing interests.

459

460 **References**

461 [1] Gupta, A. & Manthiram, A. Designing Advanced Lithium-Based Batteries for Low-
462   Temperature Conditions. *Advanced Energy Materials* **2020**, 10, 2001972.

463 [2] Zhang, S. S.; Xu, K.; Jow, T. R. The Low Temperature Performance of Li-Ion Batteries.
464   *Journal of Power Sources* **2003**, *115* (1), 137–140.

465 [3] Smart, M. C.; Ratnakumar, B. V.; Chin, K. B.; Whitcanack, L. D. Lithium-Ion Electrolytes
466   Containing Ester Cosolvents for Improved Low Temperature Performance. *J. Electrochem.*
467   *Soc.* **2010**, *157* (12), A1361–A1374.

468 [4] Li, Q.; Jiao, S.; Luo, L.; Ding, M. S.; Zheng, J.; Cartmell, S. S.; Wang, C.-M.; Xu, K.; Zhang,
469   J.-G.; Xu, W. Wide-Temperature Electrolytes for Lithium-Ion Batteries. *ACS Appl. Mater.*
470   *Interfaces* **2017**, *9* (22), 18826–18835.

471 [5] Smart, M. C.; Ratnakumar, B. V.; Ewell, R. C.; Surampudi, S.; Puglia, F. J.; Gitzendanner, R.
472   The Use of Lithium-Ion Batteries for JPL's Mars Missions. *Electrochimica Acta* **2018**, *268*,
473   27–40.

474 [6] Liu, J.; Bao, Z.; Cui, Y.; Dufek, E. J.; Goodenough, J. B.; Khalifah, P.; Li, Q.; Liaw, B. Y.;
475   Liu, P.; Manthiram, A.; Meng, Y. S.; Subramanian, V. R.; Toney, M. F.; Viswanathan, V.
476   V.; Whittingham, M. S.; Xiao, J.; Xu, W.; Yang, J.; Yang, X.-Q.; Zhang, J.-G. Pathways for
477   Practical High-Energy Long-Cycling Lithium Metal Batteries. *Nat Energy* **2019**, *4* (3), 180–
478   186.

479 [7] Xu, W.; Wang, J.; Ding, F.; Chen, X.; Nasybulin, E.; Zhang, Y.; Zhang, J.-G. Lithium Metal
480   Anodes for Rechargeable Batteries. *Energy Environ. Sci.* **2014**, *7* (2), 513–537.

481 [8] Li, S.; Jiang, M.; Xie, Y.; Xu, H.; Jia, J.; Li, J. Developing High-Performance Lithium Metal
482   Anode in Liquid Electrolytes: Challenges and Progress. *Advanced Materials* **2018**, *30* (17),
483   1706375.

484 [9] Thenuwara, A. C.; Shetty, P. P.; McDowell, M. T. Distinct Nanoscale Interphases and
485   Morphology of Lithium Metal Electrodes Operating at Low Temperatures. *Nano Lett.* **2019**,
486   *19* (12), 8664–8672.

487 [10] Thenuwara, A. C.; Shetty, P. P.; Kondekar, N.; Sandoval, S. E.; Cavallaro, K.; May, R.;
488   Yang, C.-T.; Marbella, L. E.; Qi, Y.; McDowell, M. T. Efficient Low-Temperature Cycling
489   of Lithium Metal Anodes by Tailoring the Solid-Electrolyte Interphase. *ACS Energy Lett.*
490   **2020**, *5* (7), 2411–2420.

491 [11] Dong, X.; Lin, Y.; Li, P.; Ma, Y.; Huang, J.; Bin, D.; Wang, Y.; Qi, Y.; Xia, Y. High-
492   Energy Rechargeable Metallic Lithium Battery at −70 °C Enabled by a Cosolvent
493   Electrolyte. *Angewandte Chemie International Edition* **2019**, *58* (17), 5623–5627.

494 [12] Cheng, H.; Sun, Q.; Li, L.; Zou, Y.; Wang, Y.; Cai, T.; Zhao, F.; Liu, G.; Ma, Z.; Wahyudi,
495   W.; Li, Q.; Ming, J. Emerging Era of Electrolyte Solvation Structure and Interfacial Model
496   in Batteries. *ACS Energy Lett.* **2022**, *7* (1), 490–513.

497 [13] Hou, X.-K.; Li, S.-F.; Li, W.-H.; Liang, H.-J.; Gu, Z.-Y.; Luo, X.-X.; Wu, X.-L. Electrolyte
498   Chemistry Towards Improved Cycling Stability in Na-Based Dual-Ion Batteries with High-
499   Power/Energy Storage. *Batteries & Supercaps* **2021**, *4* (10), 1647–1653.

500 [14] Liang, H.-J.; Gu, Z.-Y.; Zhao, X.-X.; Guo, J.-Z.; Yang, J.-L.; Li, W.-H.; Li, B.; Liu, Z.-M.;
501   Li, W.-L.; Wu, X.-L. Ether-Based Electrolyte Chemistry Towards High-Voltage and Long-
502   Life Na-Ion Full Batteries. *Angewandte Chemie International Edition* **2021**, *60* (51), 26837–
503   26846.

504 [15] Rustomji, C. S.; Yang, Y.; Kim, T. K.; Mac, J.; Kim, Y. J.; Caldwell, E.; Chung, H.; Meng,
505   Y. S. Liquefied Gas Electrolytes for Electrochemical Energy Storage Devices. *Science* **2017**,
506   *356* (6345), eaal4263.

507 [16] Fan, X.; Ji, X.; Chen, L.; Chen, J.; Deng, T.; Han, F.; Yue, J.; Piao, N.; Wang, R.; Zhou, X.;
508   Xiao, X.; Chen, L.; Wang, C. All-Temperature Batteries Enabled by Fluorinated Electrolytes
509   with Non-Polar Solvents. *Nature Energy* **2019**, *4* (10), 882–890.

510 [17] Wang, C.-Y.; Zhang, G.; Ge, S.; Xu, T.; Ji, Y.; Yang, X.-G.; Leng, Y. Lithium-Ion Battery
511   Structure That Self-Heats at Low Temperatures. *Nature* **2016**, *529* (7587), 515–518.

512 [18] Ji, Y.; Wang, C. Y. Heating Strategies for Li-Ion Batteries Operated from Subzero
513   Temperatures. *Electrochimica Acta* **2013**, *107*, 664–674.

514 [19] Dong, X.; Guo, Z.; Guo, Z.; Wang, Y.; Xia, Y. Organic Batteries Operated at −70°C. *Joule*
515   **2018**, *2* (5), 902–913.

516 [20] Smart, M. C.; Lucht, B. L.; Dalavi, S.; Krause, F. C.; Ratnakumar, B. V. The Effect of
517   Additives upon the Performance of MCMB/LiNixCo1−xO2 Li-Ion Cells Containing Methyl
518   Butyrate-Based Wide Operating Temperature Range Electrolytes. *J. Electrochem. Soc.*
519   **2012**, *159* (6), A739–A751.

520 [21] Zhang, J.; Zhang, J.; Liu, T.; Wu, H.; Tian, S.; Zhou, L.; Zhang, B.; Cui, G. Towards Low-
521   Temperature Lithium Batteries: Advances and Prospects of Unconventional Electrolytes.
522   *Advanced Energy and Sustainability Research.* **2021**.

523 [22] Li, Q.; Lu, D.; Zheng, J.; Jiao, S.; Luo, L.; Wang, C.-M.; Xu, K.; Zhang, J.-G.; Xu, W. Li+-
524   Desolvation Dictating Lithium-Ion Battery's Low-Temperature Performances. *ACS Appl.*
525   *Mater. Interfaces* **2017**, *9* (49), 42761–42768.

526 [23] Holoubek, J.; Liu, H.; Wu, Z.; Yin, Y.; Xing, X.; Cai, G.; Yu, S.; Zhou, H.; Pascal, T. A.;
527   Chen, Z.; Liu, P. Tailoring Electrolyte Solvation for Li Metal Batteries Cycled at Ultra-Low
528   Temperature. *Nature Energy* **2021**, *6* (3), 303–313.

529 [24] Wang, Z.; Sun, Z.; Shi, Y.; Qi, F.; Gao, X.; Yang, H.; Cheng, H.-M.; Li, F. Ion-Dipole
530   Chemistry Drives Rapid Evolution of Li Ions Solvation Sheath in Low-Temperature Li
531   Batteries. *Advanced Energy Materials*. **2021.**

532 [25] Yamada, Y.; Wang, J.; Ko, S.; Watanabe, E.; Yamada, A. Advances and Issues in
533   Developing Salt-Concentrated Battery Electrolytes. *Nat Energy* **2019**, *4* (4), 269–280.

534 [26] Wang, J.; Yamada, Y.; Sodeyama, K.; Chiang, C. H.; Tateyama, Y.; Yamada, A.
535   Superconcentrated Electrolytes for a High-Voltage Lithium-Ion Battery. *Nature*
536   *Communications* **2016**, *7* (1), 12032.

537 [27] Fan, X.; Chen, L.; Ji, X.; Deng, T.; Hou, S.; Chen, J.; Zheng, J.; Wang, F.; Jiang, J.; Xu, K.;
538   Wang, C. Highly Fluorinated Interphases Enable High-Voltage Li-Metal Batteries. *Chem*
539   **2018**, *4* (1), 174–185.

540 [28] Chen, S.; Zheng, J.; Mei, D.; Han, K. S.; Engelhard, M. H.; Zhao, W.; Xu, W.; Liu, J.;
541   Zhang, J.-G. High-Voltage Lithium-Metal Batteries Enabled by Localized High-
542   Concentration Electrolytes. *Advanced Materials* **2018**, *30* (21), 1706102.

543 [29] Ren, X.; Zou, L.; Cao, X.; Engelhard, M. H.; Liu, W.; Burton, S. D.; Lee, H.; Niu, C.;
544   Matthews, B. E.; Zhu, Z.; Wang, C.; Arey, B. W.; Xiao, J.; Liu, J.; Zhang, J.-G.; Xu, W.
545   Enabling High-Voltage Lithium-Metal Batteries under Practical Conditions. *Joule* **2019**, *3*
546   (7), 1662–1676.

547 [30] Niu, C.; Lee, H.; Chen, S.; Li, Q.; Du, J.; Xu, W.; Zhang, J.-G.; Whittingham, M. S.; Xiao,
548   J.; Liu, J. High-Energy Lithium Metal Pouch Cells with Limited Anode Swelling and Long
549   Stable Cycles. *Nat Energy* **2019**, *4* (7), 551–559.

550 [31] Wang, J.; Huang, W.; Pei, A.; Li, Y.; Shi, F.; Yu, X.; Cui, Y. Improving Cyclability of Li
551   Metal Batteries at Elevated Temperatures and Its Origin Revealed by Cryo-Electron
552   Microscopy. *Nat Energy* **2019**, *4* (8), 664–670.

553 [32] Wang, H.; Kim, S. C.; Rojas, T.; Zhu, Y.; Li, Y.; Ma, L.; Xu, K.; Ngo, A. T.; Cui, Y.
554   Correlating Li-Ion Solvation Structures and Electrode Potential Temperature Coefficients. *J.*
555   *Am. Chem. Soc.* **2021**, *143* (5), 2264–2271.

556 [33] Ueno, K.; Yoshida, K.; Tsuchiya, M.; Tachikawa, N.; Dokko, K.; Watanabe, M. Glyme–
557   Lithium Salt Equimolar Molten Mixtures: Concentrated Solutions or Solvate Ionic Liquids?
558   *J. Phys. Chem. B* **2012**, *116* (36), 11323–11331.

559 [34] Ren, X.; Zou, L.; Jiao, S.; Mei, D.; Engelhard, M. H.; Li, Q.; Lee, H.; Niu, C.; Adams, B.
560   D.; Wang, C.; Liu, J.; Zhang, J.-G.; Xu, W. High-Concentration Ether Electrolytes for Stable
561   High-Voltage Lithium Metal Batteries. *ACS Energy Lett.* **2019**, *4* (4), 896–902.

562 [35] Fadel, E. R.; Faglioni, F.; Samsonidze, G.; Molinari, N.; Merinov, B. V.; Iii, W. A. G.;
563   Grossman, J. C.; Mailoa, J. P.; Kozinsky, B. Role of Solvent-Anion Charge Transfer in
564   Oxidative Degradation of Battery Electrolytes. *Nature Communications* **2019**, *10* (1), 3360.

565   [36] Adams, B. D.; Zheng, J.; Ren, X.; Xu, W.; Zhang, J.-G. Accurate Determination of
566   Coulombic Efficiency for Lithium Metal Anodes and Lithium Metal Batteries. *Advanced*
567   *Energy Materials 8* (7), 1702097.

568   [37] Qian, J.; Henderson, W. A.; Xu, W.; Bhattacharya, P.; Engelhard, M.; Borodin, O.; Zhang,
569   J.-G. High Rate and Stable Cycling of Lithium Metal Anode. *Nature Communications* **2015**,
570   *6*, 6362.

571   [38] Marcus, R. A. On the Theory of Electron-Transfer Reactions. VI. Unified Treatment for
572   Homogeneous and Electrode Reactions. *J. Chem. Phys.* **1965**, *43* (2), 679–701.

573   [39] Newton, M. D.; Sutin, N. Electron Transfer Reactions in Condensed Phases. *Annual Review*
574   *of Physical Chemistry* **1984**, *35* (1), 437–480.

575   [40] Chidsey, C. E. D. Free Energy and Temperature Dependence of Electron Transfer at the
576   Metal-Electrolyte Interface. *Science* **1991**, *251* (4996), 919–922.

577   [41] Derr, D. L.; Elliott, C. M. Temperature Dependence of the Outer-Sphere Reorganization
578   Energy. *J. Phys. Chem. A* **1999**, *103* (39), 7888–7893.

579   [42] Nazmutdinov, R.; Quaino, P.; Colombo, E.; Santos, E.; Schmickler, W. A Model for the
580   Effect of Ion Pairing on an Outer Sphere Electron Transfer. *Phys. Chem. Chem. Phys.* **2020**,
581   *22* (25), 13923–13929.

582   [43] Perez Beltran, S.; Cao, X.; Zhang, J.-G.; Balbuena, P. B. Localized High Concentration
583   Electrolytes for High Voltage Lithium–Metal Batteries: Correlation between the Electrolyte
584   Composition and Its Reductive/Oxidative Stability. *Chem. Mater.* **2020**, *32* (14), 5973–
585   5984.

586   [44] Boyle, D. T.; Kong, X.; Pei, A.; Rudnicki, P. E.; Shi, F.; Huang, W.; Bao, Z.; Qin, J.; Cui,
587   Y. Transient Voltammetry with Ultramicroelectrodes Reveals the Electron Transfer Kinetics
588   of Lithium Metal Anodes. *ACS Energy Lett.* **2020**, *5* (3), 701–709.

589   [45] Huang, B.; Myint, K. H.; Wang, Y.; Zhang, Y.; Rao, R. R.; Sun, J.; Muy, S.; Katayama, Y.;
590   Corchado Garcia, J.; Fraggedakis, D.; Grossman, J. C.; Bazant, M. Z.; Xu, K.; Willard, A. P.;
591   Shao-Horn, Y. Cation-Dependent Interfacial Structures and Kinetics for Outer-Sphere
592   Electron-Transfer Reactions. *J. Phys. Chem. C* **2021**, *125* (8), 4397–4411.

593   [46] Baskin, A.; Lawson, J. W.; Prendergast, D. Anion-Assisted Delivery of Multivalent Cations
594   to Inert Electrodes. *J. Phys. Chem. Lett.* **2021**, *12* (18), 4347–4356.

595   [47] Asl, H. Y.; Manthiram, A. Reining in Dissolved Transition-Metal Ions. *Science* **2020**, *369*
596   (6500), 140–141.

597   [48] National Aeronautics and Space Administration. Space Technology Research Grants, Lunar
598   Surface Technology Research Opportunities Appendix. **2020**.

599   [49] Towns, J.; Cockerill, T.; Dahan, M.; Foster, I.; Gaither, K.; Grimshaw, A.; Hazlewood, V.;
600   Lathrop, S.; Lifka, D.; Peterson, G. D.; Roskies, R.; Scott, J. R.; Wilkins-Diehr, N. XSEDE:
601   Accelerating Scientific Discovery. *Computing in Science Engineering* **2014**, *16* (5), 62–74.